



A. M. Ribau · L. L. Ferrás · M. L. Morgado · M. Rebelo ·
F. T. Pinho · A. M. Afonso

Analytical study of the annular flow of a generalised Phan-Thien–Tanner fluid

Received: 14 July 2023 / Revised: 13 October 2023 / Accepted: 23 October 2023 / Published online: 7 December 2023
© The Author(s) 2023

Abstract The annular flow of complex viscoelastic fluids, described by the generalised Phan-Thien–Tanner model, is studied. This model considers the Mittag-Leffler function instead of the usual linear or exponential functions of the trace of the stress tensor, and includes two new parameters that provide additional fitting flexibility. We derive a semi-analytical solution that provides a better understanding of the behaviour of this type of fluid in annular flows and also helps to improve the modelling of complex materials.

1 Introduction

Viscoelastic materials, such as polymer melts, polymer solutions, and biofluids (e.g. blood, saliva, proteins) have complex behaviour. To better model and understand their rheological behaviour, several constitutive equations have been proposed in the literature. In this study, we consider the study of annular fluid flows that are commonly encountered in industrial processes such as drilling, cable coating, and food processing. In these processes, the fluids are mixtures of various substances, such as water, particles, oils, and other long-chain molecules, that impart the fluid with various non-Newtonian properties.

A. M. Ribau (✉) · F. T. Pinho · A. M. Afonso

Centro de Estudos de Fenómenos de Transporte, Departamento de Engenharia Mecânica, Faculdade de Engenharia, Universidade do Porto, Rua Dr. Roberto Frias, s/n, 4200-465 Porto, Portugal
E-mail: angelaribau@fe.up.pt

L. L. Ferrás
Department of Mechanical Engineering - FEUP, University of Porto, Porto, Portugal

L. L. Ferrás
CMAT - Centre of Mathematics, University of Minho, Braga, Portugal

M. L. Morgado
Center for Computational and Stochastic Mathematics, Instituto Superior Técnico, Universidade de Lisboa, Lisboa, Portugal

M. L. Morgado
Department of Mathematics, University of Trás-os-Montes e Alto Douro, UTAD, 5001-801 Vila Real, Portugal

M. Rebelo
Center for Mathematics and Applications (NOVA Math) and Department of Mathematics, NOVA FCT, Quinta da Torre, 2829-516 Caparica, Portugal

A. M. Ribau · F. T. Pinho · A. M. Afonso
ALiCE - Associate Laboratory in Chemical Engineering, Faculdade de Engenharia, Universidade do Porto, Rua Dr. Roberto Frias, s/n, 4200-465 Porto, Portugal

The literature has many analytical and numerical solutions for annular flows using different constitutive rheological models or different boundary conditions [1–11]. Among them, all the different variants of the Phan-Thien–Tanner (PTT) model have already been studied (linear, quadratic, exponential), except for the more recent PTT model, which uses the Mittag-Leffler function and is called the generalized Phan-Thien–Tanner (gPTT) model [12]. The gPTT model considers the Mittag-Leffler function instead of the classical linear and exponential functions of the trace of the stress tensor (linear PTT and exponential PTT, respectively) to ensure a much wider rheology coverage range and uses two new fitting constants to provide such additional fitting flexibility to the description of the rheological properties of viscoelastic fluids.

Using this constitutive equation, in this work we propose a new approach by deriving a new semi-analytical solution for the annular flow domain. Note that this model was previously studied for Couette and pressure-driven flows, and also in combined electro-osmotic/pressure-driven flows (see [13–15]). The obtained solutions allow the characterization of the velocity profile in annuli and can be used to validate the numerical methods and results.

The remainder of this paper is organized as follows: the next section presents the governing equations, followed by the new analytical solution in Sect. 3, the discussion of the results in Sect. 4 and the closure of the paper in Sect. 5.

2 Formulation and governing equations

We consider the pressure-driven annular flow of a viscoelastic gPTT fluid, as shown in Fig. 1, where R is the radius of the outer cylinder and aR is the radius of the inner cylinder.

The equations governing the flow of an isothermal incompressible fluid are the continuity equation

$$\nabla \cdot \mathbf{u} = 0, \quad (1)$$

and the linear momentum equation

$$\rho \frac{D\mathbf{u}}{Dt} = -\nabla p + \nabla \cdot \boldsymbol{\sigma}, \quad (2)$$

where \mathbf{u} is the velocity vector, $\frac{D}{Dt}$ is the material derivative, p is the pressure, t is the time, ρ is the fluid density and $\boldsymbol{\sigma}$ is the extra-stress tensor.

2.1 Constitutive equation

In order to achieve a closed system of equations, a constitutive equation for the extra-stress tensor, $\boldsymbol{\sigma}$, must be defined. Recently, Ferrás et al. [12] proposed a new differential rheological model based on the Phan-Thien–Tanner constitutive equation (PTT model [16,17]), derived from the Lodge–Yamamoto type of network theory for polymeric fluids. This new model considers a more general function for the rate of

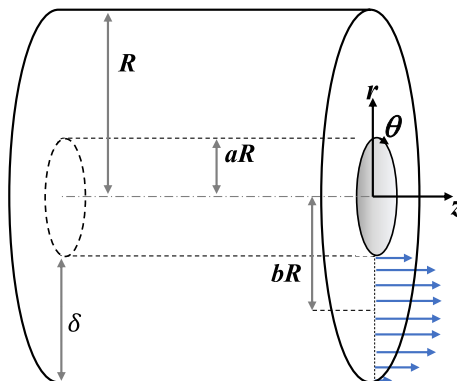


Fig. 1 Schematic of the flow in an annular region

destruction of junctions, the Mittag-Leffler function, where two fitting constants are included, in order to achieve additional fitting flexibility [12]. More details about this model are discussed in [12].

The Mittag-Leffler function is defined by

$$E_{\alpha,\beta}(z) = \sum_{j=0}^{\infty} \frac{z^j}{\Gamma(\alpha j + \beta)}, \quad (3)$$

where α, β are real and positive values and Γ is the Gamma function. When $\alpha = \beta = 1$, the Mittag-Leffler function reduces to the exponential function, and when $\beta = 1$ the original one-parameter Mittag-Leffler function, E_{α} , is obtained [18].

The constitutive equation of the gPTT model is given by

$$K(\sigma_{kk})\boldsymbol{\sigma} + \lambda \overset{\square}{\boldsymbol{\sigma}} = 2\eta_p \mathbf{D}, \quad (4)$$

where σ_{kk} is the trace of the extra stress tensor, λ is the relaxation time and η_p is the polymeric viscosity coefficient. \mathbf{D} is the rate of deformation tensor and function $K(\sigma_{kk})$ is given by

$$K(\sigma_{kk}) = \Gamma(\beta) E_{\alpha,\beta} \left(\frac{\varepsilon \lambda}{\eta_p} \sigma_{kk} \right), \quad (5)$$

where the normalization $\Gamma(\beta)$ is used to ensure that $K(0) = 1$ for all choices of β , and ε represents the extensibility parameter. $\overset{\square}{\boldsymbol{\sigma}}$ represents the Gordon-Schowalter derivative, defined as

$$\overset{\square}{\boldsymbol{\sigma}} = \frac{\partial \boldsymbol{\sigma}}{\partial t} + \mathbf{u} \cdot \nabla \boldsymbol{\sigma} - (\nabla \mathbf{u})^T \cdot \boldsymbol{\sigma} - \boldsymbol{\sigma} \cdot (\nabla \mathbf{u}) + \xi (\boldsymbol{\sigma} \cdot \mathbf{D} + \mathbf{D} \cdot \boldsymbol{\sigma}), \quad (6)$$

where $\nabla \mathbf{u}$ is the velocity gradient and the constant parameter ξ accounts for the slip between the molecular network and the continuum.

3 Semi-analytical solution for the gPTT model in annuli

We derive the analytical solution for the gPTT model considering a steady fully-developed pressure-driven annular flow (cf. Fig. 1). We consider a unidirectional flow in cylindrical coordinates, where the outer radius is R and the inner radius is aR , with $0 < a < 1$. Therefore, the momentum equation, Eq. (2), simplifies to

$$\frac{1}{r} \frac{d}{dr} (r \sigma_{rz}) = P_z, \quad (7)$$

where $P_z \equiv \frac{dp}{dz}$ is the constant streamwise pressure gradient and σ_{rz} is the shear stress.

In order to obtain closed form analytical solutions the slip parameter in the Gordon-Schowalter derivative, Eq. (6), was set to $\xi = 0$. So, the constitutive equation for the gPTT model in this flow (Sect. 2.1) can be further simplified, leading to:

$$K(\sigma_{kk})\sigma_{zz} = 2\lambda \dot{\gamma} \sigma_{rz}, \quad (8)$$

$$K(\sigma_{kk})\sigma_{rr} = 0, \quad (9)$$

$$K(\sigma_{kk})\sigma_{rz} = \eta_p \dot{\gamma}, \quad (10)$$

where the velocity gradient $\dot{\gamma}$ is a function of r ($\dot{\gamma}(r) \equiv \frac{du}{dr}$) and $\sigma_{kk} = \sigma_{\theta\theta} + \sigma_{zz} + \sigma_{rr}$ is the trace of the extra stress tensor. Under fully-developed flow conditions, $\sigma_{\theta\theta} = 0$ and $\sigma_{rr} = 0$, the trace of the extra stress tensor becomes $\sigma_{kk} = \sigma_{zz}$.

Integration of the momentum equation results in

$$\sigma_{rz} = \frac{P_z}{2} r + \frac{c}{r}, \quad (11)$$

where c is a constant of integration. Assuming that $\sigma_{rz} = 0$ at $r = bR$ (the location of the maximum velocity, see Fig. 1), with $a < b < 1$, we calculate the integration constant ($c = -(P_z/2)b^2R^2$), resulting in the following shear stress distribution,

$$\sigma_{rz} = \frac{-P_z b R}{2} \left(\frac{b R}{r} - \frac{r}{b R} \right). \tag{12}$$

Dividing Eq. (8) by Eq. (10) results in the following relationship between normal and shear stresses,

$$\sigma_{zz} = \frac{2\lambda}{\eta_p} \sigma_{rz}^2. \tag{13}$$

Solving Eq. (8) for $\dot{\gamma}$, and using Eqs. (12) and (13) results in the following velocity gradient distribution:

$$\frac{du}{dr} = -\frac{\Gamma(\beta)}{\eta_p} \frac{P_z b R}{2} \left(\frac{b R}{r} - \frac{r}{b R} \right) E_{\alpha,\beta} \left(\frac{2\varepsilon\lambda^2}{\eta_p^2} \left(\frac{P_z b R}{2} \left(\frac{b R}{r} - \frac{r}{b R} \right) \right)^2 \right). \tag{14}$$

The velocity gradient can be written in dimensionless form, using the Weissenberg number, $Wi = \lambda U_c / \delta$, where $U_c = -P_z \delta^2 / \eta_p$ is a characteristic velocity of the flow and δ is the gap between the two cylinders in the annulus. We also define $\bar{u} = u / U_c$ as the dimensionless velocity and $\bar{r} = r / \delta$ as the normalized radius/distance between the inner and outer cylinders ($\bar{R} = R / \delta$). This gives the following dimensionless velocity gradient:

$$\frac{d\bar{u}}{d\bar{r}} = \frac{\Gamma(\beta)}{2} \left(\frac{b^2 \bar{R}^2}{\bar{r}} - \bar{r} \right) E_{\alpha,\beta} \left(\frac{\varepsilon Wi^2}{2} \left(\frac{b^2 \bar{R}^2}{\bar{r}} - \bar{r} \right)^2 \right). \tag{15}$$

Now, we can obtain the velocity profile numerically by solving the following nonlinear problem:

Problem 1 Given εWi^2 and a , find the value of b that satisfies,

$$\int_{a\bar{R}}^{\bar{R}} \frac{d\bar{u}}{d\bar{r}} d\bar{r} = 0. \tag{16}$$

Using the value of b , compute the velocity profile:

$$\bar{u}(\bar{r}) = \int_{a\bar{R}}^{\bar{r}} \frac{\Gamma(\beta)}{2} \left(\frac{b^2 \bar{R}^2}{\bar{r}} - \bar{r} \right) E_{\alpha,\beta} \left(\frac{\varepsilon Wi^2}{2} \left(\frac{b^2 \bar{R}^2}{\bar{r}} - \bar{r} \right)^2 \right) d\bar{r}, \tag{17}$$

where $0 < a < 1$ is defined by the user. Equation (17) results from the no-slip boundary condition, $\bar{u}(\bar{R}) = 0$. The velocity profile in Eq. (17) can be easily approximated numerically by a simple quadrature rule. The solution of Eq. (16) can be obtained by defining $F(b) = \int_{a\bar{R}}^{\bar{R}} \frac{d\bar{u}}{d\bar{r}} d\bar{r}$. So, there exists $0 < a < b < 1$ such that $F(b) = 0$.

Equation (15) can be further expanded using the definition of the Mittag-Leffler function, resulting in

$$\frac{d\bar{u}}{d\bar{r}} = \frac{\Gamma(\beta)}{2} \left(\frac{b^2 \bar{R}^2}{\bar{r}} - \bar{r} \right) \sum_{j=0}^{\infty} \frac{1}{\Gamma(\alpha j + \beta)} \left(\frac{\varepsilon Wi^2}{2} \left(\frac{b^2 \bar{R}^2}{\bar{r}} - \bar{r} \right)^2 \right)^j \tag{18}$$

$$= \frac{\Gamma(\beta)}{2} \sum_{j=0}^{\infty} \frac{1}{\Gamma(\alpha j + \beta)} \left(\frac{\varepsilon Wi^2}{2} \right)^j \left(\frac{b^2 \bar{R}^2}{\bar{r}} - \bar{r} \right)^{2j+1} \tag{19}$$

and the velocity profile can be obtained from the integration of each term in this sum, leading to the following expression:

$$\bar{u}(\bar{r}) = \frac{\Gamma(\beta)}{2} \sum_{j=0}^{\infty} \frac{1}{\Gamma(\alpha j + \beta)} \left(\frac{\varepsilon Wi^2}{2} \right)^j \int_{a\bar{R}}^{\bar{r}} \left(\frac{b^2 \bar{R}^2}{\bar{r}} - \bar{r} \right)^{2j+1} d\bar{r} \tag{20}$$

The integral $\int \left(\frac{A}{\bar{r}} - \bar{r}\right)^{2j+1} d\bar{r}$, with $A = b^2 \bar{R}^2$, can be easily computed, using the Newton's binomial. So, the velocity profile, is given by:

$$\bar{u}(\bar{r}) = \frac{\Gamma(\beta)}{2} \sum_{j=0}^{\infty} \frac{1}{\Gamma(\alpha j + \beta)} \left(\frac{\varepsilon Wi^2}{2}\right)^j \left[\sum_{k=0}^{2j+1} \binom{2j+1}{k} \int_{a\bar{R}}^{\bar{r}} \left(\frac{b^2 \bar{R}^2}{\bar{r}}\right)^{2j+1-k} (-\bar{r})^k d\bar{r} \right] \tag{21}$$

that can be rewritten as:

$$\bar{u}(\bar{r}) = \frac{\Gamma(\beta)}{2} \sum_{j=0}^{\infty} \frac{1}{\Gamma(\alpha j + \beta)} \left(\frac{\varepsilon Wi^2}{2}\right)^j \left[\sum_{k=0}^{2j+1} \binom{2j+1}{k} (-1)^k (b^2 \bar{R}^2)^{2j+1-k} f_{kj}(a, \bar{r}) \right] \tag{22}$$

where:

$$f_{kj}(a, \bar{r}) = \begin{cases} \ln\left(\frac{\bar{r}}{a\bar{R}}\right), & \text{if } k = j. \\ \frac{\bar{r}^{2(k-j)} - (a\bar{R})^{2(k-j)}}{2(k-j)}, & \text{if } k \neq j. \end{cases} \tag{23}$$

Although Eq. (22) is an infinite series, we can obtain an approximated solution with a fair number of correct decimal places by using only $j = 3$ or $j = 4$ (depending on the problem and the parameters used). This will be explored in detail in the next section.

The second relevant problem from a practical point of view is the corresponding inverse problem of determining the pressure gradient for a given flow rate. In this second case, the following equation must be solved,

$$U = \frac{1}{\pi R^2(1 - a^2)} \int_{aR}^R u(r) 2\pi r dr \tag{24}$$

where $\pi R^2(1 - a^2)$ is the cross section area of the annular region and U is the average velocity in the annular region. Equation (24) in dimensionless form becomes:

$$\frac{2}{\bar{R}^2(1 - a^2)} \int_{a\bar{R}}^{\bar{R}} \bar{u}(\bar{r}) \bar{r} d\bar{r} - \frac{U}{U_c} = 0 \tag{25}$$

In this scenario, we can formulate the next problem:

Problem 2 Given εWi_U^2 ($Wi_U = \lambda U/\delta$) and a , find b and εWi^2 such that,

$$\bar{u}(\bar{R}) = 0 \quad \wedge \quad \frac{2}{\bar{R}^2(1 - a^2)} \int_{a\bar{R}}^{\bar{R}} \bar{u}(\bar{r}) \bar{r} d\bar{r} - \frac{U}{U_c} = 0. \tag{26}$$

Then use the values of b and εWi^2 to compute the velocity profile given by Eq. (22). Note that $U/U_c = Wi_U/Wi$.

4 Results and discussion

4.1 Assessment of the series solution

In this subsection, we compare the numerical solution of the velocity profile given by Eq. (17), with the analytical solution of Eq. (22). These results were obtained using the *Mathematica* software and we first consider a high-precision numerical solution, where we obtain the value of b using the secant method and then we numerically integrate Eq. (15). This highly accurate numerical solution of the velocity profile was then used as a reference to perform an investigation of the influence of the number of terms in the series on the error of the solution. The new truncated solution is obtained from Eq. (22), truncating the sum with $j + 1$ terms. We considered 200 equidistant mesh points along the cylinder gap and measured the maximum relative error obtained at these points (boundaries excluded). The error is calculated by $\frac{|\bar{u}(\bar{r})_{num} - \bar{u}(\bar{r})_t|}{\bar{u}(\bar{r})_{num}}$, where $\bar{u}(\bar{r})_{num}$ is the

Table 1 Maximum relative errors (in percentage) for $\varepsilon Wi^2 = 0.05$

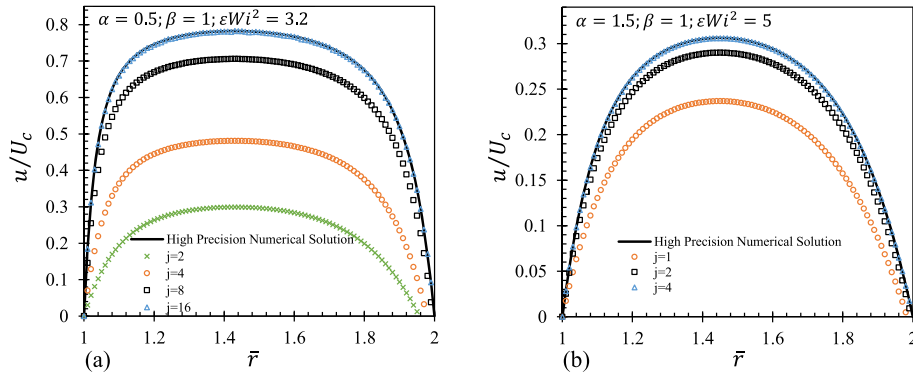
j	$\alpha = 0.5$	$\alpha = 1.5$
1	5.669×10^{-1}	9.405×10^{-2}
2	1.342×10^{-2}	4.757×10^{-4}
4	4.550×10^{-4}	4.432×10^{-4}

Table 2 Maximum relative errors (in percentage) for $\varepsilon Wi^2 = 3.2$

j	$\alpha = 0.5$
2	1.782×10^2
4	1.580×10^2
8	5.874×10^1
16	8.681×10^{-1}

Table 3 Maximum relative errors (in percentage) for $\varepsilon Wi^2 = 5$

j	$\alpha = 1.5$
1	1.414×10^2
2	4.773×10^1
4	1.409×10^0
8	4.275×10^{-4}

**Fig. 2** Velocity profiles for $\beta = 1$, $\alpha = 0.5, 1.5$ and two different values of εWi^2 , 3.2 and 5. **a** $\alpha = 0.5$; **b** $\alpha = 1.5$

approximate value of the velocity and $\bar{u}(\bar{r})_j$ is the velocity value from the truncated series. Three different values of εWi^2 were considered: 0.05, 3.2 and 5. We set $\beta = 1$ and tested two different values of α , 0.5 and 1.5. We only changed the values of α , because this parameter induces more changes in the series. The value of a used was 0.5 in all cases.

In Table 1, we show the maximum relative errors, in percentage. For $\varepsilon Wi^2 = 0.05$, the error was low, even when considering a single term in the series [Eq. (22)]. For $\alpha = 1.5$ we see that the error is much smaller, with the decrease in error becoming less pronounced as the number of terms in the series increases. This is due to the number of significant digits considered.

Tables 2 and 3 show the maximum relative errors in percentage for $\varepsilon Wi^2 = 3.2$ and 5, respectively. As we increase εWi^2 , the series solution shows convergence problems, and as we increase α (see Table 3), the error decreases faster as the number of terms in the series increases (note also that in this case we even consider a higher εWi^2 value). The corresponding velocity profiles are shown in Fig. 2, where u/U_c is the velocity profile normalised by the characteristic velocity, using the highly accurate numerical solution. These particular results indicate that the velocity profile converges to the correct profile as the number of terms in the series increases, and that this convergence is slower for low values of α .

Based on these observations, we will consider $j = 15$ for the results presented next.

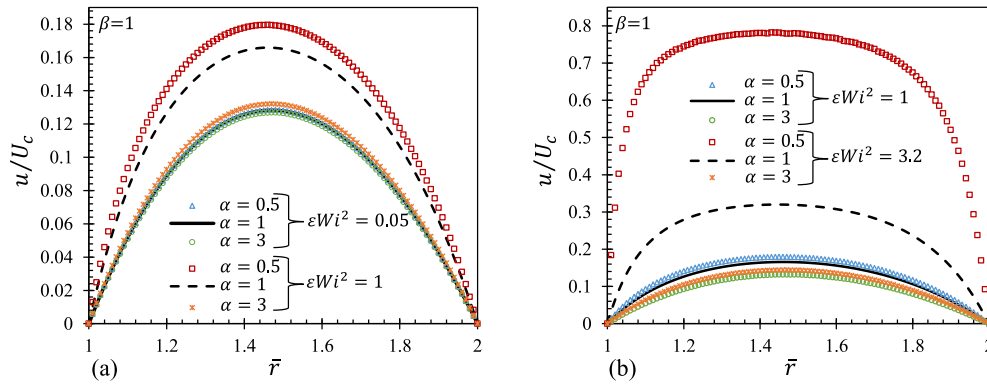


Fig. 3 Velocity profiles for $\beta = 1$, $\alpha = 0.5, 1$ and 3 . **a** $\epsilon Wi^2 = 0.05$ and 1 ; **b** $\epsilon Wi^2 = 1$ and 3.2

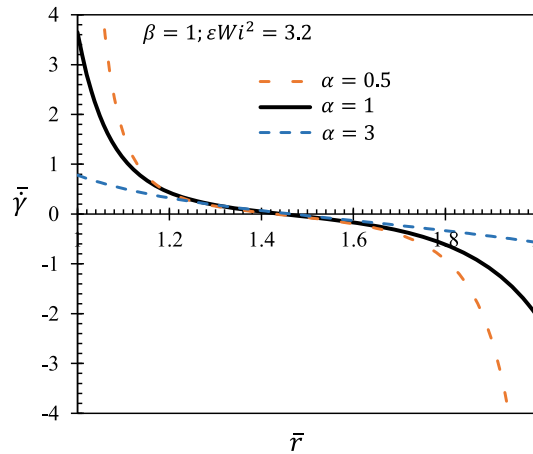


Fig. 4 Normalized shear rate profiles for $\epsilon Wi^2 = 3.2$ and $\alpha = 0.5, 1$ and 3

4.2 Problem 1

Figure 3 shows the velocity profiles for $\beta = 1$, $\alpha = 0.5, 1, 3$ at three different values of the ϵWi^2 of 0.05, 1 and 3.2.

For $\epsilon Wi^2 = 0.05$ (Fig. 3a) the velocity profiles for different values of α almost overlap. However, when we increase ϵWi^2 to 1, that no longer happens, in fact we obtain the highest velocity and flow rate for $\alpha = 0.5$, the case in which we have the highest rate of destruction of junctions. This behaviour is more pronounced when we increase elasticity (see Fig. 3b). For $\epsilon Wi^2 = 3.2$, the differences in the flow rates are obvious, except for $\alpha = 3$, where the velocity profile almost overlaps with the case $\epsilon Wi^2 = 1$. It is interesting to see that for $\alpha = \beta = 1$ we still have a parabolic velocity profile typical of Newtonian fluids, while decreasing α we observe a very pronounced plug-like profile, which is more typical of shear-thinning fluids.

To understand the slope variation of the velocity profile across the cylinder gap (for different α values), we also plotted the corresponding normalized shear rate, in Fig. 4. This way we have an idea of how much higher shear rates near the wall are for low values of α .

Figures 5a, b show the normalized shear and normal stress profiles, for $\beta = 1$, $\alpha = 0.5, 1$ and 3 for $\epsilon Wi^2 = 3.2$. For the three cases, the dimensionless normal stress is always positive and the dimensionless shear stress shows a quasi-linear profile, being positive near the inner cylinder and negative in the vicinity of the outer cylinder. The shear stress is smaller for low values of α since the values of b decrease with decreasing α (see also Eq. (15)).

Figures 6a, b and c show the influence of β on the velocity profile. The results are similar to those for the variation of α . For a small value of ϵWi^2 (Fig. 6a), the velocity profiles almost overlap for all values of β , but as ϵWi^2 is increased (Fig. 6b, c), the velocity and the flow rate increase as we decrease β . That effect is more pronounced for small values of β .

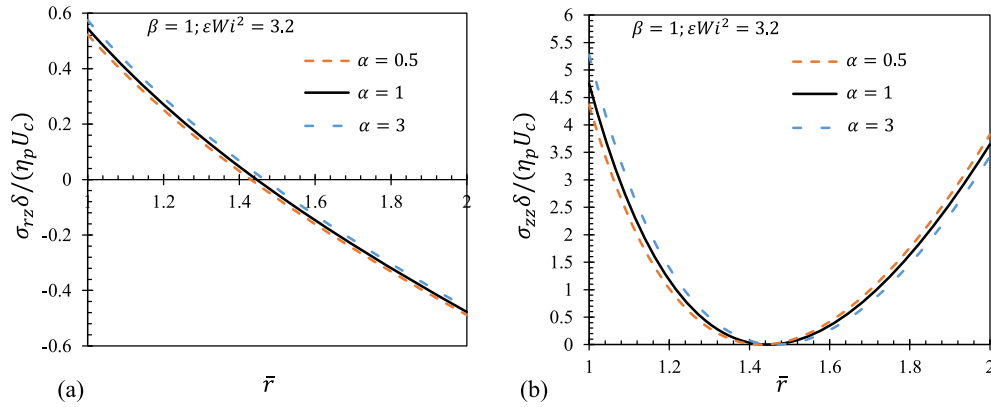


Fig. 5 Normalized shear and normal stress profiles, for $\beta = 1$, $\alpha = 0.5, 1$ and 3 and $\epsilon Wi^2 = 3.2$. **a** Normalized shear stress; **b** normalized normal stress

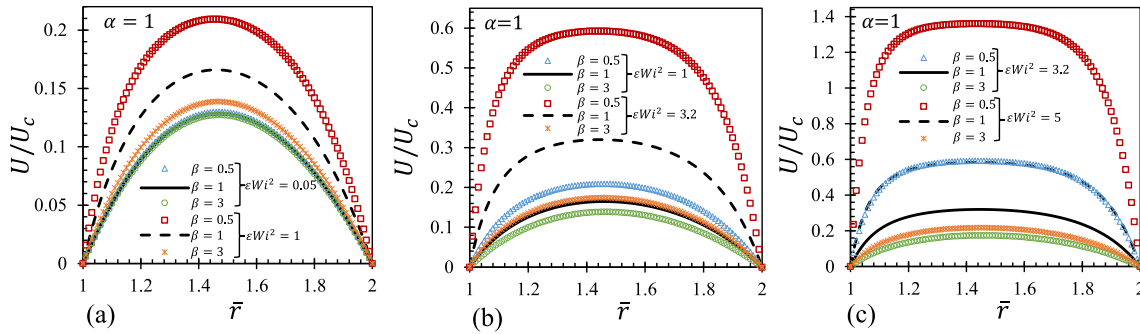


Fig. 6 Velocity profiles for $\alpha = 1$, $\beta = 0.5, 1$ and 3 ; **a** $\epsilon Wi^2 = 0.05$ and 1 ; **b** $\epsilon Wi^2 = 1$ and 3.2 ; **c** $\epsilon Wi^2 = 3.2$ and 5

The role of β is more complex than that of α . β is used as an argument of the Mittag-Leffler function and to normalize $K(\sigma_{zz})$. This mixed effect of β on the rate of destruction of junctions results in smoother variations of velocity due to the variation of β .

We also study the variations of b with ϵWi^2 (see Fig. 7). We considered three different values of α , $0.5, 1$ and 3 and calculated b for different ϵWi^2 . We see that the value of b decreases with the increase of ϵWi^2 , and that for $\alpha = 3$, the variation is almost linear. Notice that, when $\alpha = 0.5$, the reduction is more pronounced. Figure 7 shows that b decreases with the increase of the fluid elasticity, a trend also observed on the velocities profiles of Fig. 6, since the b represents the radial position of the maximum value for the velocity profile. Therefore, the point of maximum velocity approaches the inner cylinder wall as the elasticity of the fluid increases, because of the direct relationship between elasticity and shear-thinning of the shear viscosity.

4.3 Problem 2

This problem is harder to solve because for a given value of the flow rate, U , we have to find b and ϵWi^2 ($\epsilon Wi^2 = \epsilon (\lambda U_c / \delta)^2 = \epsilon (-\lambda \delta P_z / \eta_p)^2$) from a system of two strongly nonlinear equations. The first equation come from the outer wall boundary condition,

$$\frac{\Gamma(\beta)}{2} \sum_{j=0}^{\infty} \frac{1}{\Gamma(\alpha j + \beta)} \left(\frac{\epsilon Wi^2}{2}\right)^j \left[\sum_{k=0}^{2j+1} \binom{2j+1}{k} (-1)^k (b^2 \bar{R}^2)^{2j+1-k} [f_{kj}(a, \bar{R})] \right] = 0; \quad (27)$$

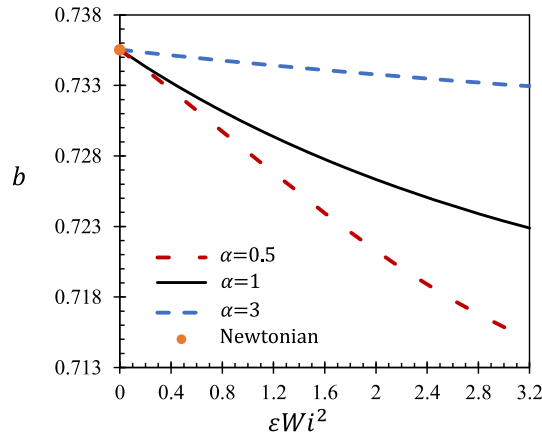


Fig. 7 Variation of b with the variation εWi^2 , for $\alpha = 0.5, 1$ and 3 . The closed circle corresponds to value of b obtained for a Newtonian fluid [1, 19]

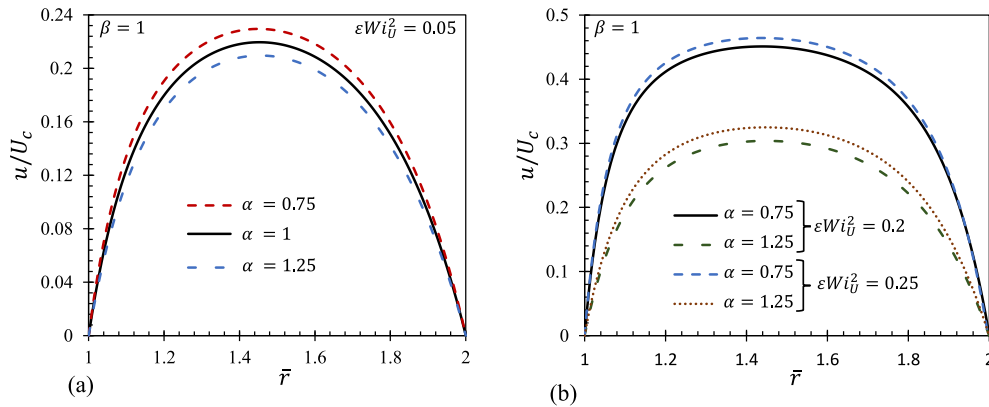


Fig. 8 Normalized velocity profiles for $\beta = 1$ and $\alpha = 0.75, 1$ and 1.25 . **a** $\varepsilon Wi^2_U = 0.05$; **b** $\varepsilon Wi^2_U = 0.2$ and 0.25

and the second from the imposed non-dimensional flow rate

$$\frac{\Gamma(\beta)}{\bar{R}^2(1-a^2)} \sum_{j=0}^{\infty} \frac{1}{\Gamma(\alpha j + \beta)} \left(\frac{\varepsilon Wi^2}{2}\right)^j \left[\sum_{k=0}^{2j+1} \binom{2j+1}{k} (-1)^k (b^2 \bar{R}^2)^{2j+1-k} [h_{kj}(a, \bar{R})] \right] - \frac{Wi_U}{Wi} = 0, \tag{28}$$

where $h_{kj}(a, \bar{R}) = \bar{R} - a\bar{R}$ if $k = j$ and $h_{kj}(a, \bar{R}) = \frac{\bar{R}^{2(k-j)+1} - (a\bar{R})^{2(k-j)+1}}{2(k-j)+1}$ if $k \neq j$. Note that $U/U_c = Wi_U/Wi$, as in Eq. (26).

Since one of the goals of this work is to provide a tool for validating future numerical implementations of this constitutive model in general numerical codes, the *Mathematica* codes used to obtain the solution are provided as supplementary material.

Figure 8 shows the normalized velocity profiles for $\beta = 1, \alpha = 0.75, 1$ and $1.25, a = 0.5$, and, for three different values of εWi^2_U : 0.05, 0.2 and 0.25.

For the lowest εWi^2_U (Fig. 8a), the velocity profiles are similar, with higher velocities for lower values of α , and, the plug-like profile typical of non-Newtonian fluids is less pronounced due to the low elasticity. Again, this confirms the idea that the lower values of α lead to more plug-like profiles due to the intense shear-thinning.

This effect is more pronounced in Fig. 8b, where we compare the results for two moderate values of elasticity. The combination of a higher εWi^2_U and a lower value of α leads to a less parabolic velocity profile.

The combined effect of elasticity and parameters α and β leads to a complex relationship. Physically, we have that a higher rate of destruction of junctions in the network (lower α) allows for a faster creation of a new network. For Problem 1, this resulted in a higher flow rate, giving the idea that, this high destruction rate

results in less resistance of the flow. When the flow rate is imposed, we observe that the information from the boundary conditions travels at a slower velocity, allowing for a more plug-like profile to be possible.

5 Conclusions

We derived an analytical solution for the velocity profile in series form for the annular flow of a gPTT fluid. A semi-analytic solution is derived for the case where the flow rate is imposed.

We show the influence of the model parameters on the velocity and stress profiles. As expected, the flow velocity increases with the decrease of α and β for the same εWi^2 , resulting in a more pronounced plug-like profile. The influence of β is less pronounced due to its double influence on the proposed rate of destruction of junctions (it is a parameter of the Mittag-Leffler function and is also used as a normalization factor).

The analytical and semi-analytical solutions presented in this work are useful for the validation of CFD codes and also provide a better understanding of the model behaviour in simple shear flows.

Acknowledgements Ângela M. Ribau would like to thank FCT - Fundação para a Ciência e a Tecnologia, for financial support through scholarship SFRH/BD/143950/2019. Ângela M. Ribau, Alexandre M. Afonso and Fernando T. Pinho also acknowledge FCT for financial support through LA/P/0045/2020 (ALiCE), UIDB/00532/2020 and UIDP/00532/2020 (CEFT), funded by national funds through FCT/MCTES (PIDDAC). L.L. Ferrás would also like to thank FCT for financial support through CMAT (Centre of Mathematics of the University of Minho) projects UIDB/00013/2020 and UIDP/00013/2020. This work was also financially supported by national funds through the FCT/MCTES (PIDDAC), under the project 2022.06672.PTDC - iMAD - Improving the Modelling of Anomalous Diffusion and Viscoelasticity: solutions to industrial problems. M.L. Morgado acknowledges funding by FCT through projects UIDB/04621/2020 and UIDP/04621/2020 of CEMAT/ IST-ID, Center for Computational and Stochastic Mathematics, Instituto Superior Técnico, University of Lisbon. This work was also funded by national funds through the FCT-Fundação para a Ciência e a Tecnologia, I.P. (Portuguese Foundation for Science and Technology) under the scope of the projects UIDB/00297/2020 and UIDP/00297/2020 (Center for Mathematics and Applications). The authors would like to thank Professor Manuel A. Alves for insightful discussions on the work.

Open Access This article is licensed under a Creative Commons Attribution 4.0 International License, which permits use, sharing, adaptation, distribution and reproduction in any medium or format, as long as you give appropriate credit to the original author(s) and the source, provide a link to the Creative Commons licence, and indicate if changes were made. The images or other third party material in this article are included in the article's Creative Commons licence, unless indicated otherwise in a credit line to the material. If material is not included in the article's Creative Commons licence and your intended use is not permitted by statutory regulation or exceeds the permitted use, you will need to obtain permission directly from the copyright holder. To view a copy of this licence, visit <http://creativecommons.org/licenses/by/4.0/>.

Funding Open access funding provided by FCTIFCCN (b-on).

References

1. Pinho, F.T., Oliveira, P.J.: Axial annular flow of a nonlinear viscoelastic fluid-an analytical solution. *J. Nonnewton. Fluid Mech.* **93**(2–3), 325–337 (2000)
2. Ferrás, L.L., Afonso, A.M., Alves, M.A., Nóbrega, J.M., Pinho, F.T.: Annular flow of viscoelastic fluids: analytical and numerical solutions. *J. Nonnewton. Fluid Mech.* **212**, 80–91 (2014)
3. Escudier, M.P., Oliveira, P.J., Pinho, F.T.: Fully developed laminar flow of purely viscous non-Newtonian liquids through annuli, including the effects of eccentricity and inner-cylinder rotation. *Int. J. Heat Fluid Flow* **23**(1), 52–73 (2002)
4. Escudier, M.P., Oliveira, P.J., Pinho, F., Smith, S.: Fully developed laminar flow of non-Newtonian liquids through annuli: comparison of numerical calculations with experiments. *Exp. Fluids* **33**(1), 101–111 (2002)
5. Bhatnagar, R.K.: Steady laminar flow of visco-elastic fluid through a pipe and through an annulus with suction or injection at the walls. *J. Indian Inst. Sci.* **45**(4), 127 (1963)
6. Cruz, D.O.A., Pinho, F.T.: Skewed Poiseuille–Couette flows of sPTT fluids in concentric annuli and channels. *J. Nonnewton. Fluid Mech.* **121**(1), 1–14 (2004)
7. Mostafaiyan, M., Khodabandehlou, K., Sharif, F.: Analysis of a viscoelastic fluid in an annulus using Giesekus model. *J. Nonnewton. Fluid Mech.* **118**(1), 49–55 (2004)
8. Mirzazadeh, M., Escudier, M.P., Rashidi, F., Hashemabadi, S.H.: Purely tangential flow of a PTT-viscoelastic fluid within a concentric annulus. *J. Nonnewton. Fluid Mech.* **129**(2), 88–97 (2005)
9. Ravanchi, M.T., Mirzazadeh, M., Rashidi, F.: Flow of Giesekus viscoelastic fluid in a concentric annulus with inner cylinder rotation. *Int. J. Heat Fluid Flow* **28**(4), 838–845 (2007)
10. Mohseni, M.M., Rashidi, F.: Analysis of axial annular flow for viscoelastic fluid with temperature dependent properties. *Int. J. Therm. Sci.* **120**, 162–174 (2017)
11. Ferrás, L.L., Afonso, A.M., Alves, M.A., Nóbrega, J.M., Pinho, F.T.: Analytical and numerical study of the electro-osmotic annular flow of viscoelastic fluids. *J. Colloid Interface Sci.* **420**, 152–157 (2014)
12. Ferrás, L.L., Morgado, M.L., Rebelo, M., McKinley Gareth, H., Afonso, A.M.: A generalised Phan-Thien–Tanner model. *J. Nonnewton. Fluid Mech.* **269**, 88–99 (2019)

13. Ribau, A.M., Ferrás, L.L., Morgado, M.L., Rebelo, M., Afonso, A.M.: Semi-analytical solutions for the Poiseuille–Couette flow of a generalised Phan-Thien–Tanner fluid. *Fluids* **4**, 129 (2019)
14. Ribau, A.M., Ferrás, L.L., Morgado, M., Rebelo, M., Afonso, A.M.: Analytical and numerical studies for slip flows of a generalised Phan-Thien–Tanner fluid. *ZAMM-J. Appl. Math. Mech./Zeitschrift für Angewandte Mathematik und Mechanik* (2020), 100(3)
15. Ribau, A.M., Ferrás, L.L., Morgado, M.L., Rebelo, M., Alves, M.A., Pinho, F.T., Afonso, A.M.: A study on mixed electro-osmotic/pressure-driven microchannel flows of a generalised Phan-Thien–Tanner fluid. *J. Eng. Math.* **127**(1), 1–15 (2021)
16. Phan-Thien, N., Tanner, R.: A new constitutive equation derived from network theory. *J. Nonnewton. Fluid Mech.* **2**, 353–365 (1977)
17. Phan-Thien, N.: A nonlinear network viscoelastic model. *J. Rheol.* **22**(3), 259–283 (1978)
18. Gorenflo, R., Kilbas, A.A., Mainardi, F., Rogosin, S.V.: *Mittag-Leffler Functions, Related Topics and Applications*. Springer, New York (2020)
19. Bird, R.B., Stewart, W.E., Lightfoot, E.N.: *Transport Phenomena*. Wiley, New York (1960)

Publisher's Note Springer Nature remains neutral with regard to jurisdictional claims in published maps and institutional affiliations.